

Dynamic modeling and structural reliability of an aeroelastic launch vehicle

Seid H. Pourtakdoust* and A.H. Khodabakhsh^a

Center for Research and Development in Space Science and Technology, Sharif University of Technology,
Tehran, 145888 9694, Iran

(Received June 27, 2021, Revised June 7, 2022, Accepted June 10, 2022)

Abstract. The time-varying structural reliability of an aeroelastic launch vehicle subjected to stochastic parameters is investigated. The launch vehicle structure is under the combined action of several stochastic loads that include aerodynamics, thrust as well as internal combustion pressure. The launch vehicle's main body structural flexibility is modeled via the normal mode shapes of a free-free Euler beam, where the aerodynamic loadings on the vehicle are due to force on each incremental section of the vehicle. The rigid and elastic coupled nonlinear equations of motion are derived following the Lagrangian approach that results in a complete aeroelastic simulation for the prediction of the instantaneous launch vehicle rigid-body motion as well as the body elastic deformations. Reliability analysis has been performed based on two distinct limit state functions, defined as the maximum launch vehicle tip elastic deformation and also the maximum allowable stress occurring along the launch vehicle total length. In this fashion, the time-dependent reliability problem can be converted into an equivalent time-invariant reliability problem. Subsequently, the first-order reliability method, as well as the Monte Carlo simulation schemes, are employed to determine and verify the aeroelastic launch vehicle dynamic failure probability for a given flight time.

Keywords: dynamic modeling; extreme response; flexible; FORM; launch vehicle; reliability

1. Introduction

Advances in high-performance lighter-weight multistage launch vehicles (LVs) have led to more flexible structures, larger thrust-to-weight, and bigger fineness ratios. Therefore, aeroelasticity plays an important role in slender LV designs and thus can affect its structural reliability. The structural reliability of an LV is the probability that its structure will not fail while performing its required mission. The reliability-based design approach utilizes distributions for loads and strengths while traditional structural design utilizes a safety factor to the maximum anticipated load or stress experienced during the flight operation.

However, the structural reliability of an aeroelastic LV is generally time-dependent as the vehicle is subjected to dynamic loads of time-varying nature. Accordingly, reliability analysis for time-variant problems is more complicated in comparison with time-invariant problems. In time-invariant reliability problems, a few well-known schemes have been developed over time for reliability estimation that includes first and second-order reliability methods (FORM and SORM) (Yao *et al.*

*Corresponding author, Professor, E-mail: pourtak@sharif.edu

^aPh.D. Candidate, E-mail: khodabakhsh@ae.sharif.edu

2013, Zhang *et al.* 2015). In contrast, the exact time-variant reliability assessment of structural systems is more stringent. There exist two schemes for time-variant reliability assessment of structural systems based on extreme response approach (Chen and Li 2007, Hu and Du 2013) and first-passage approach (Andrieu-Renaud *et al.* 2004, Singh *et al.* 2009) proposed in the literature. In the extreme response approach, the maximum performance of the system should be calculated, while in the first-passage approach the out-crossing rates must be determined. However, most first-passage approaches are under the assumption that out-crossings are statistically independent and Poisson distributed in addition to having a complicated mathematical procedure for computations.

Among the few studies available on LV reliability; most are focused on historical data. In this respect, (Young 2007) has integrated reliability, performance, and cost of an LV system to compute its total reliability based on assumed subsystem reliabilities. The Analytic Hierarchy Process allocates reliability based on expert experience and therefore is not a preferred method. Guikema and Paté-Cornell (2004) used statistical data with the Bayesian approach on some LVs to update the probability distribution of future LVs success rate. LVs reliability estimation using historical data and success rates has been performed by Allen (2001). Finally, Raouf and Pourtakdoust (2015) have optimized the cost and reliability of a two-stage LV using heuristic algorithms. In a more recent study, Raouf *et al.* (2018) estimated the structural and system reliability of a typical jet vane thrust vector control subsystem subjected to stochastic loadings utilizing various methods. LV structural reliability has also been recently investigated by the current authors while the LV solid-fluid interaction is neglected. As the above-mentioned available literature demonstrates, the aeroelastic LV reliability problem has not been attempted yet in either static or time-varying forms. Therefore, the current study focuses on the utility of the extreme response approach for the aeroelastic reliability of a launching system for which no limiting or simplifying assumptions are needed.

The remaining parts of this paper are arranged as follows. The “Reliability Analysis” section describes the theory of structural reliability. The “Equations of Motion” section presents the Lagrangian-based aeroelastic equations of motion for a typical launching system. The “Structural Analysis” section explains the structural analysis and derivation of the applied stress. Subsequently, selected LV specifications are described in the “Launch Vehicle Specifications” section. Finally, discussion of results and concluding remarks are presented in the “Discussion of Results” and “Conclusions” sections.

2. Reliability analysis

For a time-invariant reliability problem the probability of failure can be estimated by the following integral equation (Li and Chen 2009)

$$p_f = P(g(x) < 0) = \int_{g(x) < 0} f_X(x) dx \quad (1)$$

where p_f is the probability of failure, $g(x)$ is the limit state function (LSF), $f_X(x)$ is the joint probability density function, and x is the vector of random variables (or random process). While the analytical solution of this integral (Eq. (1)) is a formidable task, there exist several simpler techniques for its determination. However, for a time-dependent reliability problem the limit state function (LSF), g is a function of some random processes and thus the *instantaneous* probability of failure, $p_f^i(t)$ can now be defined

$$p_f^i(t) = P(g(x, t) < 0) = \int_{g(x, t) < 0} f_X(x, t) dx \quad (2)$$

where t varies in the flight time interval $[0, t_{\max}]$. Eq. (2) can be solved for any time instant, t using any conventional time-invariant schemes such as FORM, SORM, etc. It should be noted that the instantaneous failure probability is different from cumulative failure probability p_f^c . The cumulative structural failure probability of the LV in the time interval $[0, t_i]$ is given by

$$p_f^c(0, t_i) = p_f^c(t_i) = P(g(x, t) < 0, \exists t \in [0, t_i]) \tag{3}$$

There are various techniques based on the out-crossing rate approach developed to solve Eq. (3). However, the out-crossing rate approach requires a complicated mathematical derivation and can be implemented under some restricting simplifying assumptions. The out-crossing rate can be defined as (Singh *et al.* 2009)

$$v^+(t) = \lim_{\Delta t \rightarrow 0} \frac{P(g(x, t) > 0 \cap g(x, t + \Delta t) \leq 0)}{\Delta t} \tag{4}$$

where $g(x, t) > 0$ means the structure is in the safe domain at t and $g(x, t + \Delta t) \leq 0$ means the structure is in the failure domain at $t + \Delta t$. The mean number of out-crossings in the time interval $[0, t_i]$ is computed as:

$$E[N^+(0, t_i)] = \int_0^{t_i} v^+(t) dt \tag{5}$$

in which $N^+(0, t_i)$ denotes the number of crossings from the safe domain to the unsafe domain in the time interval $[0, t_i]$. The cumulative probability of failure can be bounded by (Singh *et al.* 2009):

$$\max_{0 \leq t \leq t_i} p_f^i(t) \leq p_f^c(0, t_i) \leq p_f^i(0) + E[N^+(0, t_i)] \tag{6}$$

To compute the out-crossing rate, the PHI2 method can be used. The PHI2 method computes an upper bound of the cumulative probability of failure of Eq. (3). Note that the dynamic system will fail if, at any time instance, the limit state is violated. However, when no random processes are directly utilized in the problem, the limit state function only depends on the initial random variables assignments and time, due to the time-varying nature of the system dynamics. Thus the LSF can be written as $g(x(\omega_0), t)$ meaning that all trajectories are deterministically obtained in time, but are randomly initialized by ω_0 (Andrieu-Renaud *et al.* 2004). Note that $x(\omega, t)$ is a random process where ω is representing a random variable from the sample space, Ω .

It is important to note that the random variables characterized in Table 1, only get established and/or updated initially at t_0 , and as such they only change from one launch system to another as opposed to from one time to another. As an example, based on Table 1 the material strength is a variable that is randomly selected at t_0 and remains constant during the total flight time for each stage. Therefore, for the system under study the probability of failure in the time interval $[0, t_i]$ is equal to the probability of $\min g(x(\omega_0), t)$ exceeding a threshold value in the same time interval $[0, t_i]$ or

$$p_f^c(0, t_i) = P([\min g(x(\omega_0), t)] < 0, \exists t \in [0, t_i]) \tag{7}$$

Please note that the extreme response method utilized in this research has no inherent assumptions and/or simplifications (unlike other methods such as the first-passage, etc.). However if one is dealing with pure random processes, obviously other methods such as the out-crossing rate approach should be utilized (Singh *et al.* 2009).

As mentioned earlier, one can realize that the probability of having a minimum response of $g(x, t)$ in the time interval $[0, t_i]$, exceeding a threshold value is equal to the probability of failure

in that same time interval. This realization forms the basis of the extreme response approach. Utilizing this concept, the time-variant reliability problem is converted to a time-invariant one. Consider the time-dependent structural LSF as

$$g_s(x, t) = \sigma_y - \max_x \{\sigma_v(x, t)\} \quad (8)$$

where the subscript “s” corresponds to stress-related failures, σ_y is the yield strength, and $\max_x \{\sigma_v(x, t)\}$ is the maximum instantaneous Von Mises stress along the LV length. Note that $g_s(x, t) > 0$ indicates structural safety, and so $g_s(x, t) < 0$ denotes its failure. The cumulative failure probability (Eq. (3)) in time interval $[0, t_i]$ can then be estimated by (Chen and Li 2007)

$$\begin{aligned} p_f^c(0, t_i) &= P\left(\min_{0 < t < t_i} g_s(x, t) < 0, \exists t \in [0, t_i]\right) \\ &= P\left(\min_{0 < t < t_i} (\sigma_y - \max_x \{\sigma_v(x, t)\}) < 0, \exists t \in [0, t_i]\right) \\ &= P\left((\sigma_y - \max_{0 < t < t_i} \max_x \{\sigma_v(x, t)\}) < 0, \exists t \in [0, t_i]\right) \\ &= P((\sigma_y - w) < 0) \end{aligned} \quad (9)$$

where w is the extreme response of $\max_x \{\sigma_v(x, t)\}$ in each time interval,

$$w = \max_{0 < t < t_i} \left(\max_x \{\sigma_v(x, t)\}, t \in [0, t_i]\right), i = 1, 2, 3, \dots, N \quad (10)$$

Thus, applying the above analysis for each sequence time intervals, i.e., $[0, t_1]$, $[0, t_2]$, $[0, t_3]$, ..., $[0, t_{\max}]$, the time-dependent reliability problem is converted into a time-invariant one for any time intervals. Thus, a time-independent reliability method such as FORM can be applied for each time sequence. It is important to note that in this study random variables only change from one launch system to another, not from one time to another time in flight.

2.1 First-order reliability method

FORM is widely used for structural reliability estimation and is based on a linear approximation of the LSF. The accuracy of FORM depends on the level of non-linearity involved in the LSF. FORM implementation requires stochastic variables to be transformed into independent standard normal space U for which the reliability index is computed via a constrained optimization problem (Liu *et al.* 2014)

$$\begin{aligned} \beta &= \min_u \sqrt{\sum_{i=1}^n u_i^2} \\ \text{subject to } g(u) &= 0 \end{aligned} \quad (11)$$

The solution of Eq. (11) is called the most probable point and denoted by u^* . The point u^* is on the failure surface and has the shortest distance to the origin. Accordingly, the probability of failure can be calculated as

$$p_f \approx \Phi(-\beta) \quad (12)$$

where Φ is the standard normal cumulative distribution function, β (reliability index) is the distance between the origin and the u^* in the standard normal space. Though there are various

algorithms to solve Eq. (11), the Hasofer-Lind and Rackwitz-Fiessler method is used in the current study to search for the most probable point (Liu *et al.* 2014).

2.2 Direct Monte Carlo method

Monte Carlo simulation (MCS) is an attractive alternative technique for structural reliability assessment that is not limited by any simplifying assumptions whose application for reliability analysis is computationally intensive especially for stiff structures with low failure probability. However, MCS can be utilized for validation purposes of FORM and SORM. MCS requires random sample generation according to some presumed statistical distribution of the system random variables. Subsequently, cumulative failure probability is estimated as the ratio of the number of samples falling in the failure region, N_f over the total number of samples, N_s while the total samples should be large (Tang *et al.* 2013)

$$p_f^c(0, t_i) = \frac{1}{N_s} \sum_{j=1}^{N_s} k[g(x, t) \leq 0] \quad \forall t \in [0, t_i] \quad (13)$$

Or

$$p_f^c(0, t_i) = \frac{N_f}{N_s} \text{ for } N_s \rightarrow \infty \forall t \in [0, t_i] \quad (14)$$

where $k[.]$ is an indicator function defined by

$$k[g(x) \leq 0] = \begin{cases} 1 & \text{if } g(x) \leq 0 \\ 0 & \text{otherwise} \end{cases} \quad (15)$$

3. Equations of motion

For a slender elastic LV, the general local deformation vector $\vec{e} = (e_x, e_y, e_z)$ in the body-fixed coordinate system can be represented as a linear combination of normal mode shape functions, $\phi_i(x)$ (Bilimoria and Schmidt 1995, Waszak and Schmidt 1988) (Fig. 1)

$$\vec{e} = \begin{pmatrix} 0 \\ 0 \\ \sum_{i=1}^n \phi_i(x) \zeta_i(t) \end{pmatrix} \quad (16)$$

where ζ_i is the generalized coordinate. As the LV is guided in the launch plane, the lateral deformation is relatively small and thus neglected. The axial deformation is also small and neglected in this study. Besides, as the LVs are usually axisymmetric, the i^{th} mode shape (and also mass moments of inertia) in the y and z directions are equal.

The coupled rigid-elastic non-linear equations of motion can be developed using the Lagrangian approach (Bilimoria and Schmidt 1995, Shi and Zhao 2016)

$$\frac{d}{dt} \left(\frac{\partial T}{\partial \dot{q}_i} \right) - \frac{\partial T}{\partial q_i} + \frac{\partial U}{\partial q_i} + \frac{\partial D}{\partial \dot{q}_i} = Q_i \quad (17)$$

where q_i are the generalized coordinates. The relations for the kinetic energy T , potential energy U , and damping energy D are also available. Finally, assembling the governing coupled rigid-elastic LV equations of motion can be written as (Bilimoria and Schmidt 1995, Shi and Zhao 2016)

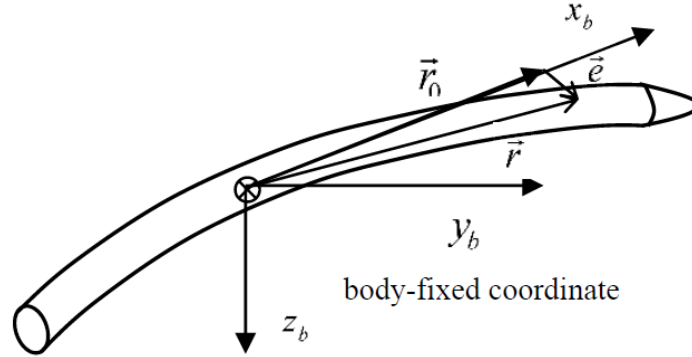


Fig. 1 General configuration of the bending LV

$$\dot{u} = \frac{F_x}{m} + rv - qw \quad (18)$$

$$\dot{v} = \frac{F_y}{m} + pw - ru \quad (19)$$

$$\dot{w} = \frac{F_z}{m} + qu - pv \quad (20)$$

where u , v , and w are the linear velocities of the body-fixed frame relative to inertia frame, p , q and r are the angular velocities of the body-fixed frame relative to inertia frame and m is the launch vehicle mass

$$\dot{p} = \frac{M_x - 2p \sum_{i=1}^n \zeta_i \dot{\zeta}_i + qr \sum_{i=1}^n \zeta_i^2}{I_x + \sum_{i=1}^n \zeta_i^2} \quad (21)$$

$$\dot{q} = \frac{M_y - pr(I_x - I + \sum_{i=1}^n \zeta_i^2) - 2q \sum_{i=1}^n \zeta_i \dot{\zeta}_i +}{I + \sum_{i=1}^n \zeta_i^2} \quad (22)$$

$$\dot{r} = \frac{M_z - pq(I - I_x)}{I} \quad (23)$$

where I_x and I are the mass moments of inertia about x and y axes of the body-fixed frame and n is the number of mode shape

$$\ddot{\zeta}_i = Q_{\zeta_i} - 2\mu_i \omega_i \dot{\zeta}_i - (\omega_i^2 - p^2 - q^2)\zeta_i \quad (24)$$

where μ_i is the critical damping ratio of the i^{th} bending mode and ω_i is the i^{th} mode natural bending frequency. The external forces (F_x, F_y, F_z) and moments (M_x, M_y, M_z) applied to the LV include the effect of the exhaust thrust forces, gravity as well as aerodynamic force distribution. The gravitational force for an elliptic Earth model is utilized as a function of the LV center of mass position (altitude). Exhaust forces and moments include the combined effect of the main thrust as a function of time and local elastic bending action on the vehicle.

$$F_{T_x} = F_T \cos(\delta + \gamma(x_T)) \approx F_T (\cos(\delta) - \sin(\delta) \sum_{i=1}^n \phi'_i(x_T) \zeta_i) \quad (25)$$

$$F_{T_z} = F_T \sin(\delta + \gamma(x_T)) \approx F_T (\sin(\delta) + \cos(\delta) \sum_{i=1}^n \phi'_i(x_T) \zeta_i) \quad (26)$$

in which δ is the engine thrust vector angle and $\gamma(x_T)$ is the elastic deflection of the LV at exhaust position such that

$$\cos(\gamma(x_T)) \approx 0, \sin(\gamma(x_T)) \approx \sum_{i=1}^n \phi'_i(x_T) \zeta_i \quad (27)$$

The normal aerodynamic force is calculated as a function of the LV local angles of attack for each incremental section via a force derivative per unit length to be integrated over the LV length (Shi and Zhao 2016)

$$F_{za} = - \int_L L_\alpha(x) \alpha(x, t) dx \quad (28)$$

where L_α is the normal aerodynamic force derivative per unit length of the LV

$$L_\alpha(x) = q_\infty A \bar{C}_{z_\alpha} \quad (29)$$

in which q_∞ is the dynamic pressure, A is the LV cross-sectional area, \bar{C}_{z_α} is the normal lift curve slope per unit length. The aerodynamic forces in x and y directions of the body-fixed frame can be computed as

$$F_{xa} = -q_\infty A C_x \quad (30)$$

$$F_{ya} = -q_\infty A C_y \quad (31)$$

The aerodynamic coefficients can be estimated from wind-tunnel tests on a rigid model or via numerical techniques. The aerodynamic moment about the y -axis is the summation of moments due to force on each incremental section of the LV.

$$M_{ya} = - \int_L x L_\alpha(x) \alpha(x, t) dx \quad (32)$$

The moment about the z -axis is calculated as

$$M_{za} = q_\infty A d C_n \quad (33)$$

In turn, the segment's local angles of attack, $\alpha(x, t)$ along the LV can be represented as follows

$$\alpha(x, t) = \alpha + \frac{1}{u} \sum_{i=1}^n \phi_i(x) \dot{\zeta}_i - \sum_{i=1}^n \phi'_i(x) \zeta_i - \frac{qx}{u} \quad (34)$$

where α is the rigid-body angle of attack. Besides, the generalized forces due to virtual displacement ζ_i is calculated as

$$Q_{\zeta_i}(t) = - \int_L L_\alpha(x) \alpha(x, t) \phi_i(x) dx + F_T \phi_i(x_T) \sum_{i=1}^n \phi'_i(x_T) \zeta_i \quad (35)$$

3. Structural analysis

To define an LSF for reliability analysis, two performance functions related to the LV sectional maximum applied stress and maximum elastic tip (nose) deformation are considered. It is assumed that the LV structure fails when either maximum applied stress or maximum elastic tip deformation exceeds a pre-specified threshold limit. Axial compression loads, moments, and stresses emanating from the pressurized solid rocket motor (SRM) are the primary loads considered for LV structural analysis and design. LVs are assumed to be guided to fly in the initial launch plane such that lateral loads could be effectively ignored. Therefore, most applied forces act in the longitudinal direction, and maximum bending stress occurs either at the outer top or bottom edges of the LV body cylindrical case. Additionally, it is assumed that a normal distributed internal pressure, P_0 is applied on the inner surface of the SRM casing during the burn time of the elastic stages.

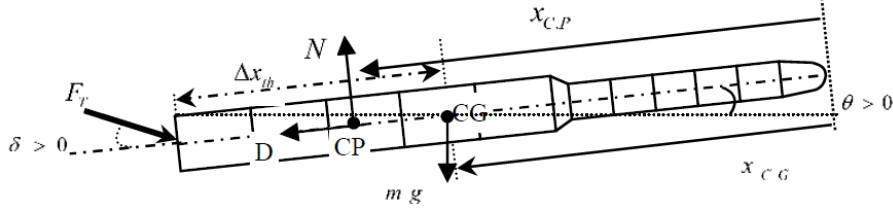


Fig. 2 Forces acting on the LV

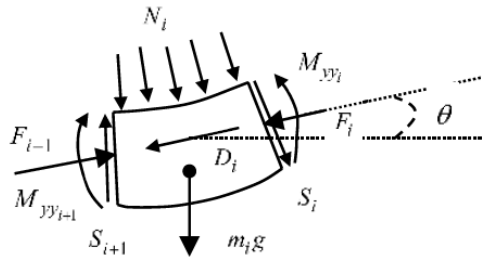


Fig. 3 The free-body diagram of the LV segment

Fig. 2 shows a typical LV with externally applied forces, where the structure is divided into 12 segments. Each segment is located at a specific position x_i as measured from the vehicle nose.

Fig. 3 also shows shear forces, bending moments, and axial loads applied on the LV segment.

Note that the compressive axial force F_i along the LV length is due to the exhaust thrust force and axial aerodynamic force. In this respect, to determine the inner axial force F_i , the LV is divided into several segments as depicted in Fig. 3 showing an arbitrary segment free-body diagram at any instant of flight time. Application of Newton's second law of motion to the differential element relates the internal axial forces to be determined (see Fig. 3).

$$F_{i+1} = F_i + D_i + m_i g \sin \theta + m_i a_{x_i} \tag{36}$$

where D_i is the axial aerodynamic force at the section i and m_i is the mass of the element at the section i . The instantaneous mass of the LV can be computed from the following relation

$$m(t) = M_0 - \frac{M_p t}{t_b} \tag{37}$$

where M_0 is the initial mass of the launch vehicle, M_p is the propellant mass, and t_b is the burning time. The net axial acceleration of each vehicle segment a_{x_i} is the sum of the LV total axial acceleration plus the segment centrifugal acceleration

$$a_{x_i} = a_x + (x_{C.G_i} - x_{C.G})\dot{\theta}^2 \tag{38}$$

Finally, the net sectional longitudinal and hoop stresses can be calculated from

$$\sigma_l(x, t) = \frac{P_0 R}{2h} - \frac{F_i(x, t)}{A} \pm \frac{M_{yy_i}(x, t) R}{I_{yy}} \tag{39}$$

$$\sigma_\theta(x, t) = \frac{P_0 R}{h} \tag{40}$$

where h and R are the thickness and radius of motor case respectively. Also, the relationship between

the internal bending moment (at any section) and elastic deflection can be written as

$$M_{yy_i}(x, t) = -EI_{yy} \frac{\partial^2 e_z(x, t)}{\partial x^2} \quad (41)$$

Substitution of Eq. (41) into Eq. (39) yields the relation for the longitudinal stress as

$$\sigma_l(x, t) = \frac{P_0 R}{2h} - \frac{F_i(x, t)}{A} \mp ER \frac{\partial^2 e_z(x, t)}{\partial x^2} \quad (42)$$

Subsequently, utilizing Eq. (16) provides the desired form of stress relations

$$\sigma_l(x, t) = \frac{P_0 R}{2h} - \frac{F_i(x, t)}{A} \mp ER \sum_{i=1}^n \zeta_i(t) \frac{d^2}{dx^2} \phi_i(x) \quad (43)$$

$$\sigma_\theta(x, t) = \frac{P_0 R}{h} \quad (44)$$

Structural failure occurs when the Von Mises stress exceeds a specified threshold value governed by the material type. Next, neglecting the radial and shear stress components, Von Mises stress at any segment is computed

$$\sigma_v(x, t) = (\sigma_l^2 - \sigma_l \sigma_\theta + \sigma_\theta^2)^{0.5} \quad (45)$$

Where σ_l and σ_θ are the longitudinal and hoop stress. Finally, the time-dependent structural LSF is determined using the following relation

$$g_s(x, t) = \sigma_y - \max_x \{\sigma_v(x, t)\} \quad (46)$$

where the subscript s corresponds to stress-related failures and $\max_x \{\sigma_v(x, t)\}$ is the maximum instantaneous Von Mises stress along the LV length. Of course, another failure mode can occur when maximum elastic tip deformation exceeds an allowable threshold e_z^* . Note that in general, the tail and tip segments experience larger deformation compared with other midsegments

$$g_d(x, t) = e_z^* - |e_z(x_N, t)| \quad (47)$$

where the subscript d denotes displacement-related failures and $e_z(x_N, t)$ denotes the vehicle tip elastic displacement. Finally, failure occurs when either $g_s(x, t) < 0$ or $g_d(x, t) < 0$. According to section 2, time-dependent LSFs can be converted to time-independent LSFs as

$$g_s(x) = \sigma_y - \max_{x,t} \{\sigma_v(x, t)\} \quad (48)$$

$$g_d(x) = e_z^* - \max_{x,t} |e_z(x_N, t)| \quad (49)$$

With this proposition, any basic time-invariant reliability method such as FORM and SORM could be utilized for time-variant reliability assessment.

4. Launch vehicle specifications

Fig. 4 shows a typical two-stage solid propellant rocket considered in this study. The main subsystems of the vehicle include the payload, guidance module, structure, and SRM case. The mission is to put a 50 kg payload into a circular low Earth orbit of 340 km altitude. The vehicle has body diameters of 3 m and 2 m for the first and second stages respectively and an overall length of 22 m. Uncertainties will occur for several design parameters that in turn affect the reliability. Table

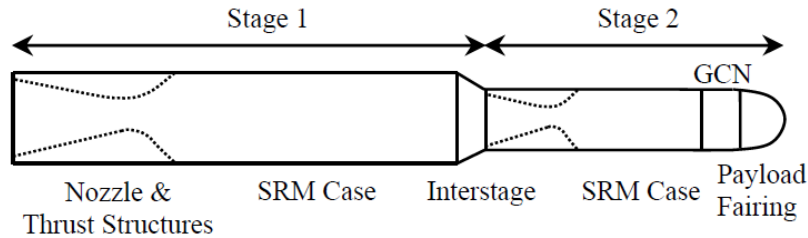


Fig. 4 General launch vehicle configuration

Table 1 Probabilistic characteristics of elastic LV

Random variables	Unit	Mean value	Coefficient of variation, %	Distribution
Mass moment of inertia, I_x	kg·m ²	5355*	2	Bounded normal
Mass moment of inertia, I	kg·m ²	396667*	2	Bounded normal
Modal damping, $\mu_i, i = 1,2,3$	-	0.02	2	Bounded normal
Equivalent bending stiffness, EI_{yy}	N·m ²	1.534×10^9	3	Bounded normal
Aerodynamic coefficients	-	**	4	Bounded normal
Specific impulse, I_{sp}	s	260	1	Bounded normal
Combustion chamber pressure, P_0	MPa	8.62	2	Bounded normal
Thrust, F_T	N	28.0×10^5	1	Bounded normal
Yield strength, σ_y	Mpa	663.9	1	Bounded normal

*At the beginning of flight

**Calculate from lookup table according to LV angle of attack, Mach number and Reynolds

1 represents uncertainties associated with the LV structure, aerodynamics, thrust, and material uncertainties.

5. Discussion of results

In this section, the time-variant reliability of an aeroelastic LV having uncertain parameters and subjected to a combination of aerodynamics, inertial, thrust, and internal combustion pressure loadings is estimated. The vehicle's rigid body motion and elastic deformations are obtained by simultaneous solution of Eqs. (18)-(24) performed using the Runge-Kutta algorithm in an in-house developed simulation tool. Fig. 5 and Fig. 6 show time variations of the LV dynamic pressure and angle of attack respectively for a nominal simulation. The LV starts an accelerated motion from a stationary initial condition. After a short-time vertical accelerated ascent trajectory, the pitch program is applied. In this stage, the dynamic pressure constantly increases to its maximum value q_{\max} as the LV's Mach increases. As the LV gains enough altitude, the air-density drops which leads to a decrease in the dynamic pressure. The first stage burns out in 60 seconds after lift-off after which the second stage is assumed to be ignited immediately. Based on the flight performance results, one can provide other results that may be useful for design and reliability analysis.

Moreover, the typical time variation of the LV tip displacement in the vertical direction is shown in Fig. 7 for the first stage. Note that this result is extracted from a single deterministic execution of the simulation code. The plot of e_z clearly demonstrates that the displacement amplitude increases

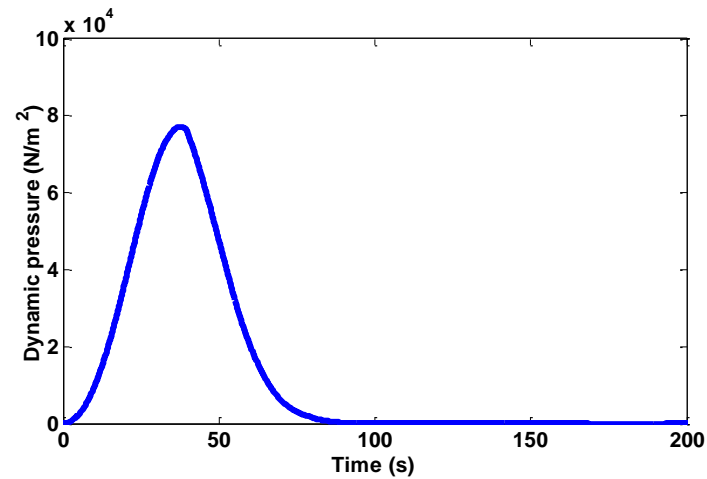


Fig. 5 Variation of dynamic pressure with time (nominal simulation)

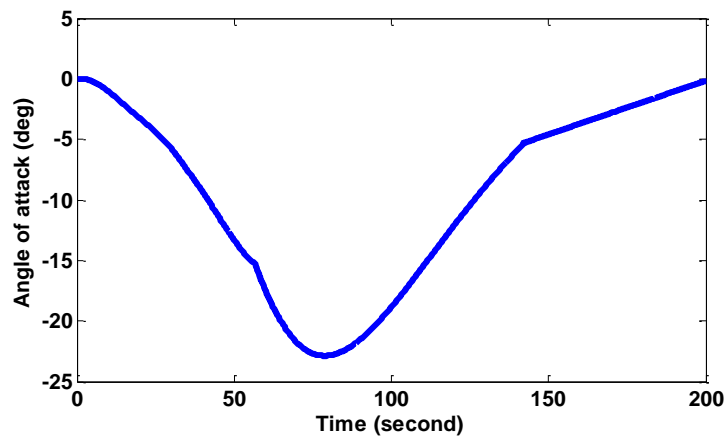


Fig. 6 Time variation of the angle of attack (nominal simulation)

in an oscillatory fashion that grows especially in the maneuvering phase. Previous research experience of the current and other authors indicated that three modes produce sufficient accuracy in elastic deformations and no significant changes are observed for higher numbers (Pourtakdoust and Assadian 2004).

The results are only plotted for stage one [0,60 s] operation since after separation the LV fineness ratio reduces, the system operates at higher less dense altitude and thus aeroelastic reliability flattens and remains constant for the remainder of the total flight time.

Cumulative structural failure probability of LV increases with time due to time-varying loads of stochastic nature such as the aerodynamics, thrust, and SRM internal pressure loadings. Subsequently, the failure occurs as the maximum applied Von Mises stress or maximum elastic tip deformation during flight exceeds a pre-specified critical threshold. In this respect, the accuracy of FORM is verified against 300,000 MCS. To verify the MCS results, the convergence of the COV (Coefficient of Variation) is presented. To this end, the L^2 -norm between the normalized consecutive MCS COVs are generated. The COVs are normalized with respect to the initial COV.

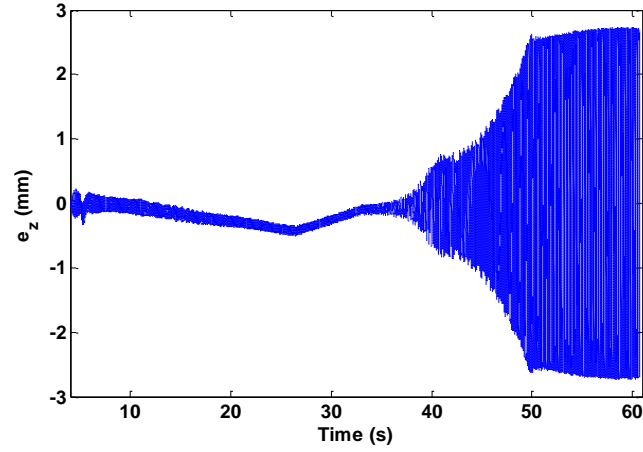


Fig. 7 Time history of the tip elastic displacement in the vertical direction (nominal simulation)

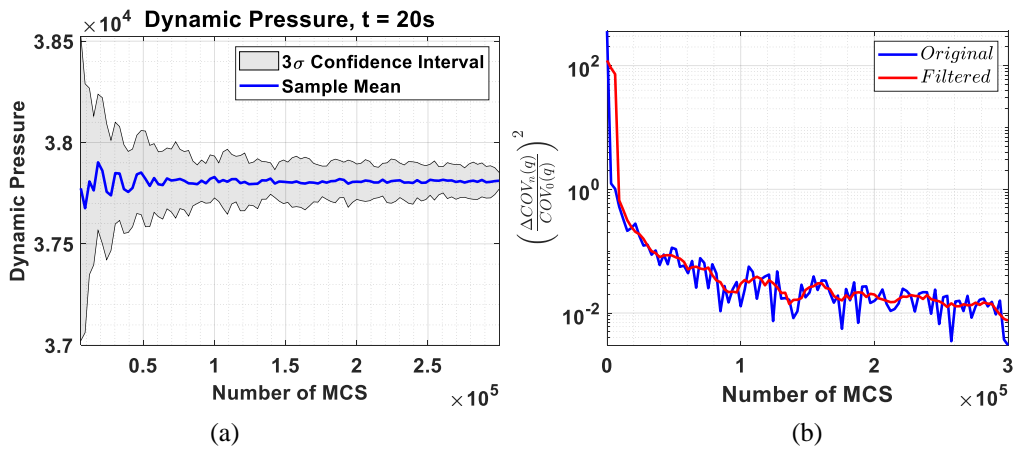


Fig. 8 Dynamic pressure MCS history, (a) confidence interval, (b) COV convergence

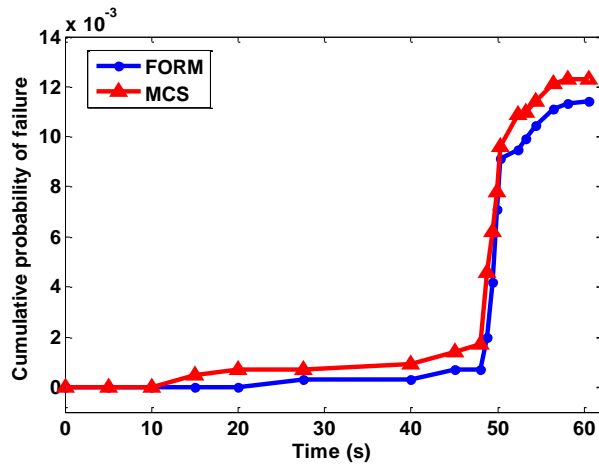


Fig. 9 Cumulative elastic displacement failure probability, p_d^c

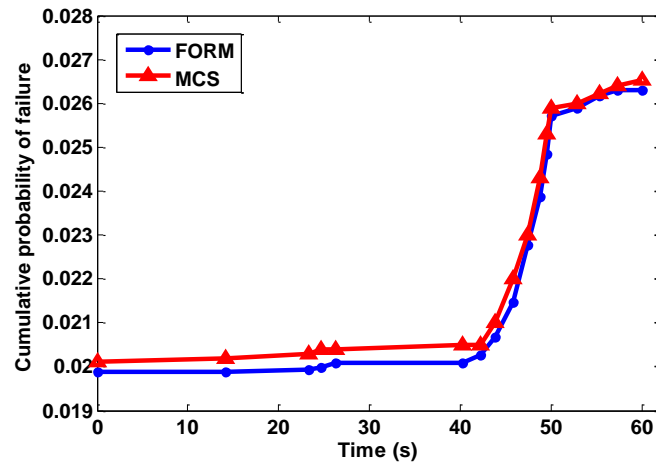


Fig. 10 Cumulative structural failure probability, p_s^c

Next, a 50-sample moving average is used to filter the computational noise and verify the convergence process of the MSC. Fig. 8 shows the MCS COV history and the confidence interval for the dynamic pressure at $t = 20s$.

The cumulative failure probability of the aeroelastic LV structure, p_s^c , and displacement, p_d^c , utilizing both FORM and MCS methods are shown in Fig. 9 and Fig. 10 respectively. As shown in Fig. 8 the value of p_d^c starts at zero initially that is maintained for 10 seconds after launch and then gradually increases with a sharp rise to a maximum around 50 seconds after launch due to LV maneuvering.

Similarly, Fig. 10 shows the p_s^c behavior utilizing FORM and MCS analysis for verification. As indicated in Fig. 10, p_s^c is not zero even at the beginning of flight due to SRM pressure loading. Moreover, the results indicate that the probability of structural failure is more than the deformation failure. Figs. 9 and 10 also demonstrate that FORM results are in good agreement with those of MCS with a maximum error of about 2.36% for the LV structure. However, it is important to note that FORM convergence is achieved only after 44 function evaluations, while MCS is converged after approximately about 300,000 simulations for each point in plots of Figs. 9 and 10. Each function evaluation for the relations given in the manuscript roughly takes about 0.673 seconds on a vintage Core i7-6700HQ. Hence, the MCS takes about 56 hours to complete. On the other hand, the FORM analysis approximately takes only about a minute to complete.

Even though the utilized extreme response method requires no additional assumption, the very small error of the FORM analysis against the MCS can be traced back to the error of the first-order approximation of the reliability integral. Note that the cumulative failure probability evolves and increases as the uncertainties associated with the LV's parameters and aerodynamic loads are applied. Subsequently, the failure associated with the maximum applied von Mises stress during flight dominates the aeroelastic deformation-based failure of the LV under study.

5. Conclusions

Time-variant reliability analysis of an aeroelastic launch vehicle system subject to stochastic

aerodynamic, inertial as well as internal ballistic loadings is investigated. The failure criteria could either be the maximum allowable stress or the maximum tip elastic deformation that occurs during the LV flight time. To this aim, the Lagrangian-based nonlinear elastic LV equations of motion are utilized where elastic displacements are modeled via normal mode shapes emanating from a Euler type beam representing the elastic LV. Subsequently, two time-dependent limit state functions (stress and deformation) are proposed to evaluate the LV cumulative failure probability via a widespread first-order reliability method whose outputs are verified through the direct Monte Carlo simulation.

It is realized that the stress-related failure probability is higher than the deformation-based failure probability for the aeroelastic LV under study. With a maximum error of about 2.36%, the FORM analysis results show good agreement with those of MCS. The results indicate that the proposed method can compute the LV time-variant reliability with good accuracy and thus can be potentially used in the LV design cycle for enhanced reliability. Future work is planned towards an integration of the aeroelastic LV structure with its other subsystems reliability to achieve the total system time-varying reliability.

Data Availability

Some or all data, models, or codes that support the findings of this study are available from the corresponding author upon reasonable request.

References

- Allen, B. (2001), "Historical reliability of US launch vehicles", *37th Joint Propulsion Conference and Exhibit*.
- Andrieu-Renaud, C., Sudret, B. and Lemaire, M. (2004), "The PHI2 method: A way to compute time-variant reliability", *Reliab. Eng. Syst. Saf.*, **84**(1), 75-86. <https://doi.org/10.1016/j.res.2003.10.005>.
- Bilimoria, K.D. and Schmidt, D.K. (1995), "Integrated development of the equations of motion for elastic hypersonic flight vehicles", *J. Guid. Control Dyn.*, **18**(1), 73-81. <https://doi.org/10.2514/3.56659>.
- Chen, J.B. and Li, J. (2007), "The extreme value distribution and dynamic reliability analysis of nonlinear structures with uncertain parameters", *Struct. Saf.*, **29**(2), 77-93. <https://doi.org/https://doi.org/10.1016/j.strusafe.2006.02.002>.
- Guikema, S.D. and Paté-Cornell, M.E. (2004), "Bayesian analysis of launch vehicle success rates", *J. Spacecraft. Rocket.*, **41**(1), 93-102. <https://doi.org/10.2514/1.9268>.
- Hu, Z. and Du, X. (2013), "A sampling approach to extreme value distribution for time-dependent reliability analysis", *J. Mech. Des.*, **135**(7), 071003. <https://doi.org/10.1115/1.4023925>.
- Li, J. and Chen, J. (2009), *Stochastic Dynamics of Structures*, John Wiley & Sons.
- Liu, J., Wang, Q., Chen, J., Zhao, H. and Duan, D. (2014), "Preliminary reliability analysis of a high-altitude airship's envelope", *Proc. Inst. Mech. Eng., Part G: J. Aerosp. Eng.*, **228**(9), 1648-1653. <https://doi.org/10.1177/0954410013499495>.
- Pourtakdoust, S. and Assadian, N. (2004), "Investigation of thrust effect on the vibrational characteristics of flexible guided missiles", *J. Sound Vib.*, **272**(1-2), 287-299. [https://doi.org/10.1016/S0022-460X\(03\)00779-X](https://doi.org/10.1016/S0022-460X(03)00779-X).
- Raouf, N. and Pourtakdoust, S.H. (2015), "Launch vehicle multi-objective reliability-redundancy optimization using a hybrid genetic algorithm-particle swarm optimization", *Proc. Inst. Mech. Eng., Part G: J. Aerosp. Eng.*, **229**(10), 1785-1797. <https://doi.org/10.1177/0954410014560381>.
- Raouf, N., Pourtakdoust, S.H. and Paghaleh, S.S. (2018), "Reliability and failure analysis of jet vane TVC

- system”, *J. Fail. Anal. Preve.*, **18**(6), 1635-1642. <https://doi.org/10.1007/s11668-018-0563-9>.
- Shi, Z. and Zhao, L. (2016), “Effects of aeroelasticity on coning motion of a spinning missile”, *Proc. Inst. Mech. Eng., Part G: J. Aerosp. Eng.*, **230**(14), 2581-2595. <https://doi.org/10.1177/0954410016629501>.
- Singh, A., Mourelatos, Z.P. and Li, J. (2009), “Design for lifecycle cost using time-dependent reliability”, *International Design Engineering Technical Conferences and Computers and Information in Engineering Conference*, **49026**, 1105-1119.
- Tang, Z., Lu, Z., Feng, J. and Wang, B. (2013), “The applications of an importance sampling method to reliability analysis of the inside flap of an aircraft”, *Proc. Inst. Mech. Eng., Part G: J. Aerosp. Eng.*, **227**(6), 916-932. <https://doi.org/10.1177/0954410012444185>.
- Waszak, M.R. and Schmidt, D.K. (1988), “Flight dynamics of aeroelastic vehicles”, *J. Aircraft*, **25**(6), 563-571. <https://doi.org/10.2514/3.45623>.
- Yao, W., Chen, X., Huang, Y. and van Tooren, M. (2013), “An enhanced unified uncertainty analysis approach based on first order reliability method with single-level optimization”, *Reliab. Eng. Syst. Saf.*, **116**, 28-37. <https://doi.org/10.1016/j.res.2013.02.014>.
- Young, D.A. (2007), “An innovative methodology for allocating reliability and cost in a lunar exploration architecture”, Georgia Institute of Technology.
- Zhang, Z., Jiang, C., Wang, G. and Han, X. (2015), “First and second order approximate reliability analysis methods using evidence theory”, *Reliab. Eng. Syst. Saf.*, **137**, 40-49. <https://doi.org/10.1016/j.res.2014.12.011>.

CC

Nomenclature

$(\cdot)_b$	= quantity represented in body-fixed coordinate	h	= thickness of the motor case
A	= cross-sectional area of the LV	$k[.]$	= Indicator function
$\bar{C}_{z\alpha}$	= normal lift curve slope per unit length	m	= launch vehicle mass
CG	= center of gravity	p_f	= probability of failure
CP	= center of pressure	p_f^c	= cumulative probability of failure
D	= damping energy	$p_f^i(t)$	= instantaneous probability of failure
D_i	= axial aerodynamic force	q_∞	= dynamic pressure
F_i	= compressive axial force	q_i	= generalized coordinated
I	= mass moment of inertia about y-axis of the body-fixed frame	\vec{r}	= position vector
I_x	= mass moment of inertia about x-axis of the body-fixed frame	t_b	= burning time
L_α	= normal aerodynamic force	w	= extreme response
M_0	= initial mass of the LV	Φ	= standard normal cumulative distribution function
M_p	= propellant mass	Ω	= sample space
M_{yy_i}	= bending moment	$\alpha(x, t)$	= angle of attack along the LV
$N^+(0, t_i)$	= number of out-crossings	β	= reliability index
N_i	= normal aerodynamic force	$\gamma(x_T)$	= Elastic deflection of the LV

N_f	= number of samples in failure region	δ	= engine thrust vector angle
N_s	= total number of samples	ζ_i	= generalized coordinate
S_i	= shear force	μ_i	= critical damping ratio of the i^{th} bending mode
T	= kinetic energy	v^+	= out-crossing rate
R	= radius of the motor case	σ_l	= sectional longitudinal stress
U	= potential energy	σ_θ	= Sectional hoop stress
\vec{e}	= General local deformation vector	$\phi_i(x)$	= normal mode-shape functions
$g(\mathbf{x})$	= limit state function	ω	= random variable
$g_s(\cdot)$	= time-dependent structural LSF		